Available online at www.sciencedirect.com

ScienceDirect

Procedia Structural Integrity 2 (2016) 1781–1788

Structural Integrity Procedia

www.elsevier.com/locate/procedia

21st European Conference on Fracture, ECF21, 20-24 June 2016, Catania, Italy

Role of vortex-like motion in fracture of coating-substrate system under contact loading

A.Yu. Smolin[a]*, G.M. Eremina[b], E.V. Shilko[a], S.G. Psakhie[c,d]

[a]*Institute of Strength Physics and Materials Science SB RAS, pr. Akademicheskiy 2/4, 634055, Tomsk, Russia*
[b]*Tomsk State University, pr. Lenina 36, 634050, Tomsk, Russia*
[c]*Tomsk Institute of High Technology Physics of Tomsk Polytechnic University, pr. Lenina 30, 634050, Tomsk, Russia*
[d]*Skolkovo Institute of Science and Technology, Novaya St., 100, Karakorum Building, 4th floor, Skolkovo, 143025, Russia*

Abstract

Deformation of a heterogeneous material containing internal interfaces or/and free surfaces is accompanied by collective vortex motion near these boundaries. One should expect that rotational motion in nanomaterials takes place at different scales, from the atomic scale to the macroscopic one. Nevertheless such a fundamental factor as elastic vortex motion in material formed during dynamic loading still remains out of discussion. The aim of this paper is revealing the role of vortex displacements in contact interaction of the strengthening coating with a hard counter-body by means of 3D modeling using movable cellular automata (MCA). MCA method is an efficient numerical method in particle mechanics, which assumes that the material is composed of a certain amount of elementary objects interacting among each other according to many-particle forces. In this paper MCA method is applied to 3D modeling deformation of the coating-substrate system under its contact loading by the rigid indenter. Main attention of the research is focused on the role of vortex structures in the velocity fields in elastic and non-elastic deformation of the strengthening coating and substrate. The mechanical properties of the model coating correspond to multifunctional nanostructured film and the properties of the substrate, to nanostructured titanium. The loading is performed by a hard conical indenter with various ratios of normal and tangential components. The peculiarities of the velocity vortex formation and propagation, as well as interaction with the structural elements are studied.

Peer-review under responsibility of the Scientific Committee of PCF 2016.

Keywords: Nanostructured coating; contact loading; elastic waves; velosity field; vortex; simulation

* Corresponding author. Tel.: +7-3822-286-975; fax: +7-3822-492-576.
E-mail address: asmolin@ispms.tsc.ru

Peer review under responsibility of the Scientific Committee of PCF 2016.
10.1016/j.prostr.2016.06.224

1. Introduction

Usually dynamic loading of solids is attended by generation and propagation of the surface elastic waves of elliptical polarization which manifest themselves as vortex structures in the velocity field (Landau and Lifshitz, 1970; Psakhie et al., 1997). Such vortex structures are also typical for the Lamb waves taking place in thin plates as shown by Chertov et al. (2004). Deformation of a heterogeneous material containing internal interfaces or/and free surfaces is accompanied by collective vortex motion near these boundaries (Panin et al., 2016; Psakhie et al., 2014b; Moiseenko et al., 2013). For example, molecular dynamics simulations by Psakh'e and Zol'nikov (1997) showed that vortex structures in the velocity field are formed at grain boundaries under shear loading of polycrystals. Therefore, one should expect that rotational motion in nanomaterials takes place at different scales from the atomic scale to the macroscopic one. The results of theoretical studies and experimental evidence by Zhang et al. (2005) indicate that in nanomaterials the contribution of rotational mode of deformation can significantly increase under the condition of dynamic loading. Nevertheless such a fundamental factor as the elastic vortex motion in material formed during dynamic loading still remains out of discussion. Thus, revealing the role of vortex displacement in redistribution of elastic energy and, as a result, in the process of deformation and fracture of nanomaterials is a topical fundamental problem in materials science.

Due to principal significance of free surface, internal interfaces and dynamic nature of the considered vortex phenomena the main method of studying them seems to be computer simulation based on particle methods (Yu et al., 2014). Therefore, the aim of this paper is revealing the role of vortex displacements in the contact interaction of strengthening coating with hard counter-body by means of 3D modeling using movable cellular automata.

2. Description of the Model

For modeling interaction of a small counter-body moving over the coating surface we used movable cellular automaton (MCA) method, which is a new efficient numerical method in particle mechanics. Within the frame of MCA, it is assumed that any material is composed of a certain amount of elementary objects (automata) which interact among each other and can rotate and move from one place to another, thereby simulating a real deformation process (Psakhie et al., 2014a; Shilko et al., 2015; Smolin et al., 2015). The automaton motion is governed by the Newton-Euler equations:

$$\begin{cases} m_i \dfrac{d^2\mathbf{R}_i}{dt^2} = \displaystyle\sum_{j=1}^{N_i} \mathbf{F}_{ij}^{\text{pair}} + \mathbf{F}_i^{\Omega}, \\ \hat{J}_i \dfrac{d\boldsymbol{\omega}_i}{dt} = \displaystyle\sum_{j=1}^{N_i} \mathbf{M}_{ij}, \end{cases} \tag{1}$$

where $\mathbf{R}_i$, $\boldsymbol{\omega}_i$, m_i and $\hat{J}_i$ are the location vector, rotation velocity, mass and moment of inertia of ith automaton, respectively; $\mathbf{F}_{ij}^{\text{pair}}$ is the interaction force of the pair of ith and jth automata; and $\mathbf{F}_i^{\Omega}$ is the volume-dependent force acting on ith automaton and depending on the interaction of its neighbors with the remaining automata. In the latter equation, $\mathbf{M}_{ij} = q_{ij}(\mathbf{n}_{ij} \times \mathbf{F}_{ij}^{\text{pair}}) + \mathbf{K}_{ij}$, where q_{ij} is the distance from the center of ith automaton to the point of its interaction ("contact") with jth automaton, $\mathbf{n}_{ij} = (\mathbf{R}_j - \mathbf{R}_i)/r_{ij}$ is the unit vector directed from the center of ith automaton to the jth one and r_{ij} is the distance between automata centers, $\mathbf{K}_{ij}$ is the torque caused by relative rotation of automata in the pair.

Note that the automata of the pair may represent the parts of different bodies or one consolidated body. Therefore its interaction is not always really contact one. That is why we put the word "contact" in quotation marks. More of that, the size of the automaton is characterized by one parameter d_i, but it does not mean that the shape of the automaton is spherical. Real shape of the automaton is determined by area of its "contacts" with neighbors. For example, if we use initial fcc packing, then the automata are shaped like a rhombic dodecahedron; but if we use cubic packing then the automata are cube-shaped.

For locally isotropic media, the volume-dependent component of the force can be expressed in terms of the pressure P_j in the volume of the neighboring automaton j as follows:

$$\mathbf{F}_i^{\Omega} = -A\sum_{j=1}^{N_i} P_j S_{ij} \mathbf{n}_{ij} \tag{2}$$

where S_{ij} is the area of interaction surface of automata i and j; and A is a material parameter depending on elastic properties.

The total force acting on automaton i can be represented as a sum of explicitly defined normal component $\mathbf{F}_{ij}^{\mathrm{n}}$ and tangential (shear) component $\mathbf{F}_{ij}^{\tau}$:

$$\mathbf{F}_i = \sum_{j=1}^{N_i} \left(\mathbf{F}_{ij}^{\mathrm{pair}} - AP_i S_{ij} \mathbf{n}_{ij} \right) = \sum_{j=1}^{N_i} \left[\left(F_{ij}^{\mathrm{pair},n}\left(h_{ij}\right) - AP_j S_{ij} \right) \mathbf{n}_{ij} + F_{ij}^{\mathrm{pair},\tau}\left(\mathbf{l}_{ij}^{\mathrm{shear}}\right) \mathbf{t}_{ij} \right] = \sum_{j=1}^{N_i} \left(\mathbf{F}_{ij}^{n} + \mathbf{F}_{ij}^{\tau} \right) \tag{3}$$

where $\mathbf{F}_{ij}^{\mathrm{pair,n}}$ and $\mathbf{F}_{ij}^{\mathrm{pair},\tau}$ are the normal and tangential pair interaction forces depending respectively on the automata overlap h_{ij} and their relative tangential displacement $\mathbf{l}_{ij}^{\mathrm{shear}}$ calculated with taking into account the rotation of both automata. Note that, although the last expression of Eq. (3) formally corresponds to the form of element interaction in conventional discrete element models, it differs fundamentally from them in many-particle central interaction of the automata.

Using the homogenization procedure for stress tensor in a particle described by Psakhie et al. (2014a), the expression for components of the average stress tensor in the automaton i takes the form:

$$\bar{\sigma}_{\alpha\beta}^{i} = \frac{1}{V_i} \sum_{j=1}^{N_i} q_{ij} n_{ij,\alpha} F_{ij,\beta} \tag{4}$$

where α and β denote the axes X, Y, Z of the global coordinate system; V_i is the current volume of the automaton i; $\mathbf{n}_{ij,\alpha}$ is the α-component of the unit vector $\mathbf{n}_{ij}$; and $F_{ij,\beta}$ is β-component of the total force acting at the point of "contact" between the automata i and j.

The interaction parameters of movable cellular automata are considered in relative (specific) units. Thus, the central and tangential interactions of the automata i and j are characterized by the corresponding stresses η_{ij} and $\boldsymbol{\tau}_{ij}$:

$$\begin{cases} F_{ij}^{n} = \eta_{ij} S_{ij} \\ \mathbf{F}_{ij}^{\tau} = \boldsymbol{\tau}_{ij} S_{ij} \end{cases}. \tag{5}$$

To characterize the deformation of the automaton i under its normal interaction with the automaton j, we can use the following dimensionless parameter (normal strain)

$$\xi_{ij} = \frac{q_{ij} - d_i/2}{d_i/2} \tag{6}$$

In general case, each automaton of a pair represents different material, and the overlap of the pair is distributed between ith and jth automata :

$$\Delta h_{ij} = \Delta q_{ij} + \Delta q_{ji} = \Delta\xi_{ij}\, d_i/2 + \Delta\xi_{ji}\, d_j/2 \tag{7}$$

where symbol Δ denotes the increment of a parameter per time step Δt of numerical integration of the motion equation (1). The distribution rule for strain in the pair is intimately associated with the expression for computing the interaction forces of the automata. This expression for central interaction is similar to Hooke's relations for diagonal stress tensor components:

$$\Delta\eta_{ij} = 2G(\Delta\xi_{ij}) + (1 - 2G/K)P_i, \tag{8}$$

where K is the bulk modulus; G is the shear modulus of the material of ith automaton; and P_i is the pressure of the automaton i, which may be computed using Eqs. (3) and (4) at previous time step or by predictor-corrector scheme.

To determine a parameter characterizing shear deformation in the pair of automata i–j, we start with formula for tangential component of rotational velocity of the pair as a rigid body

$$\boldsymbol{\omega}_{ij} = \frac{\mathbf{n}_{ij} \times (\mathbf{v}_j - \mathbf{v}_i)}{r_{ij}}. \tag{9}$$

Besides such rotation of the pair as a whole (defined by the difference in translational velocities of the automata), each automaton rotates with its own rotational velocity $\boldsymbol{\omega}_i$. The difference between these rotational velocities produces a shear deformation. Thus, the increment of shear deformations of the automata i and j per time step Δt is defined by the relative tangential displacement at the contact point $\mathbf{l}_{ij}^{\text{shear}}$:

$$\Delta\boldsymbol{\gamma}_{ij} + \Delta\boldsymbol{\gamma}_{ji} = \frac{\Delta\mathbf{l}_{ij}^{shear}}{r_{ij}} = \frac{\left(q_{ij}\left(\boldsymbol{\omega}_{ij} - \boldsymbol{\omega}_i\right) \times \mathbf{n}_{ij} + q_{ji}\left(\boldsymbol{\omega}_{ij} - \boldsymbol{\omega}_j\right) \times \mathbf{n}_{ji}\right)\Delta t}{r_{ij}}. \tag{10}$$

The expression for tangential interaction of movable cellular automata is similar to Hooke's relations for non-diagonal stress tensor components and is pure pairwise:

$$\Delta\boldsymbol{\tau}_{ij} = 2G(\Delta\boldsymbol{\gamma}_{ij}). \tag{11}$$

The difference in automaton rotation leads also to the deformation of relative “bending” and “torsion” (the last only in 3D) of the pair. It is obvious that the resistance to relative rotation in the pair cause the torque, which value is proportional to the difference between the automaton rotations:

$$\Delta\mathbf{K}_{ij} = -(G_i + G_j)(\boldsymbol{\omega}_j - \boldsymbol{\omega}_i)\Delta t. \tag{12}$$

Eqs. (1)–(8), (10)–(12) describe the mechanical behavior of a linearly elastic body in the framework of MCA method. Note that Eqs. (7), (8), (10)–(12) are written in increments, i.e., in the hypoelastic form. Psakhie et al. (2011) showed that this model gives the same results as the numerical solving usual equation of continuum mechanics for isotropic linearly elastic medium by finite-difference method. That makes it possible to couple MCA method with the numerical methods of continuum mechanics. Smolin et al. (2009) showed that the rotation allows the movable cellular automata to describe the isotropic response of material correctly.

In this paper the coating of multifunctional bioactive nanostructured film (TiCCaPON) on nanostructured titanium substrate (Levashov et al., 2013) has been modeled using approach by Psakhie et al. (2009, 2013). These materials are used in medicine for producing various kinds of implants. The thickness of the model coating is H = 60 nm, the model sample length L = 350 nm, width M = 250 nm, the size of the automata d = 3 nm (Fig. 1,a). Diamond counter-body has a conical shape with a base diameter of 60 nm. We use cubic packing of automata, which is much more suitable for studying elastic deformation of the material due to less number of automata in the model and more uniform shape of the crack-like defects. Motion of the counter-body is simulated by setting the constant

velocity $V = 5$ cm/s in the direction of axis Y for automata of the upper layer of the counter-body (Fig. 1). The lower surface of the sample is fixed and its lateral surfaces are free. Removing of automata from initial packing allows explicitly account of voids or pores in the material. Changing sort (i.e. mechanical properties) of the automata in the initial packing allows account of various kind of inhomogeneity in the material.

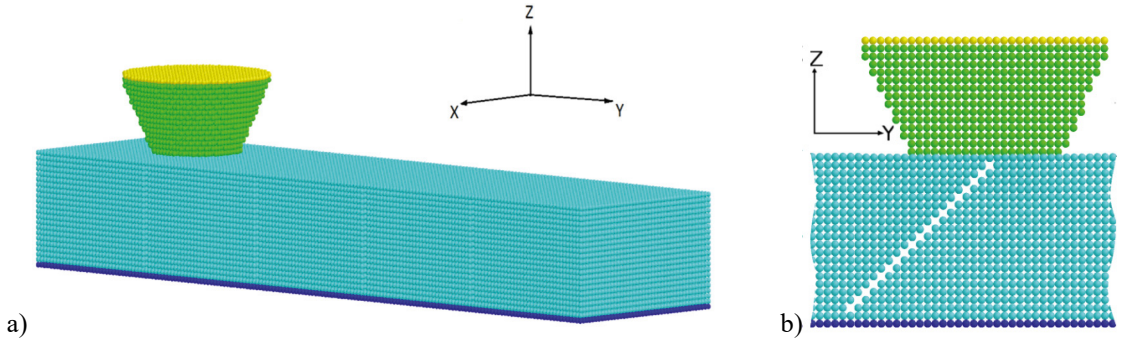

Fig. 1. General view of the modeled system (a) and cross-section of the coating with a pore (b).

3. Results of Simulation

Main attention of this research is focused on the role of vortex-like structures in the velocity fields in the strengthening coating. That is why first we studied the peculiarities of the velocity field in homogeneous coating under contact loading with hard conical counter-body moving along the free upper surface. Due to artificial roughness caused by discrete representation of the material and its surface, the movement of the counter-body along the surface with constant velocity results in periodic loading of the coating surface right in the contact patch. This cause generation of elastic waves in the coating, which propagate in the bulk and along the surface, and interact with another waves and structure elements of the material. As a result, the velocity field in the coating is drastically non-uniform and time dependent.

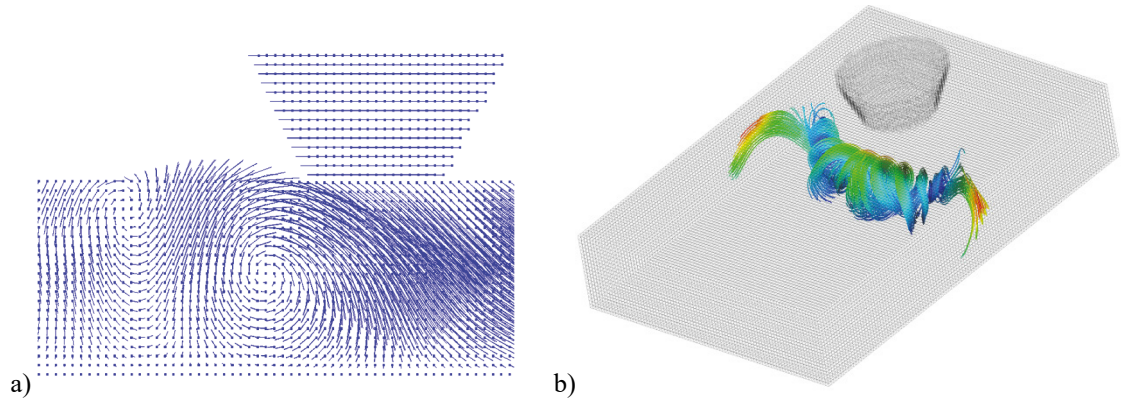

Fig. 2. Vortex in the velocities of coating particles in front of the moving counter-body shown in cross-section of the sample (a, 2D picture) and in streamlines of the velocity field in 3D (b).

Analysis of numerical 2D vector field is very easy, one can see vortices right from the picture of vectors shown as arrows or lines. Analysis of 3D vector fields is much more complicated problem. One can try to look at 2D vector fields in a series of parallel sections of the 3D body. But, to see a vortex in this case you need making sections by planes perpendicular to the vortex direction (Fig. 2,a). This means that first you need to compute the vorticity. To analyze vorticity of the 3D vector field we used post-processor software VisIt. To find vortices we plot streamlines of the velocity field at characteristic time steps (Fig. 2,b). To make the picture clearer we try different options and

select the optimal ones. Of course, the resulting streamlines show just a tendency of the particle motion at the current time step, not real trajectories like in fluid dynamics. Nevertheless, this approach allows detecting position and "power" of vortex structures in 3D vector field of velocities and therefore is quite applicable for our task.

The results of simulation show that vortices mainly occur in the corners of the coating as a result of relaxation of elastic energy near free surface where it is allowed to move in several directions. The vortex in the vicinity of counter-body is formed periodically in time in front of the counter-body. Then it becomes wider, propagates ahead and rounds the counter-body. Lifetime of such vortex structure is about 0.015 ns, which corresponds to the time of sound propagation through the coating height. The vortex size is commensurable with half of the coating height.

Then we considered the coating containing damages. The damage of the coating was simulated by specifying the extended discontinuities, nano-pores. These nano-pores were located periodically at the predetermined distance from one another and inclined to the upper surface by 45° (Fig. 1,b). In this case vortex-like motion takes place only in the material between the pores, and due to their specific geometry the vortex axis cannot round about the counter-body (Fig. 3,a). The size of the vortex is less than one in case of intact material. The vortex is generated approximately in the middle of height of the coating. Then it becomes larger, propagates towards the lower surface along the orientation of the pores, and finally is divided into two parts which start to propagate to the right and left lateral surfaces of the coating correspondingly and vanishes.

The third sample contained hard inclusions of the same geometry as the pores in the sample of second kind. Elastic properties of the inclusions are two times greater than elastic properties of the coating. Typical vortex in this sample is shown in Fig. 3,b. One can see that it is similar to the case of intact material, but a little bit smaller.

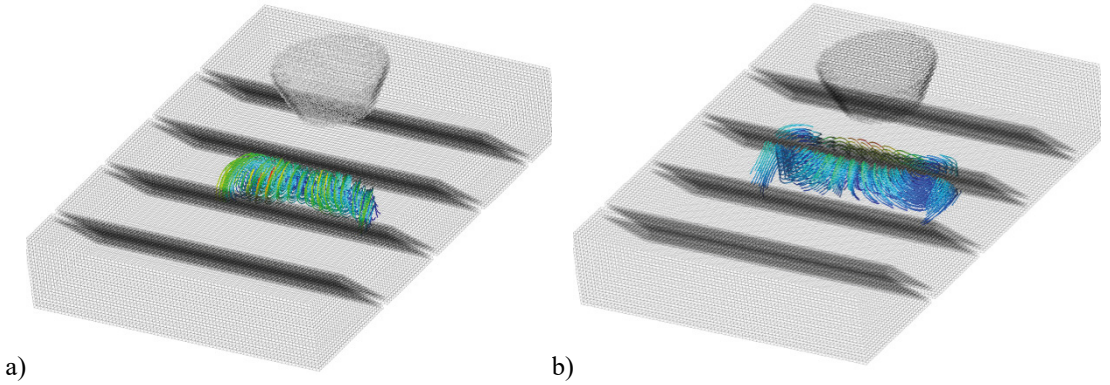

Fig. 3. Streamlines showing the vortices in the particles velocities of the coating with pores (a) and hard inclusions (b).

The next problem considered in this work was the role of vortex mechanism in the rearrangement of elastic energy in vicinity of interfaces and in the initiation of plastic deformation in nanostructured materials under contact loading. For this purpose we considered the same samples with inclusions as above but the material of inclusions was soft and could undergo plastic deformation. These inclusions imitated weak grain boundaries of a nanocrystalline material and crossed all the samples along axis *OX* i.e. in the direction transversal to the direction of counterbody motion (Fig. 1). Cross sections of the inclusions were varied in size as well in shape (Fig. 4).

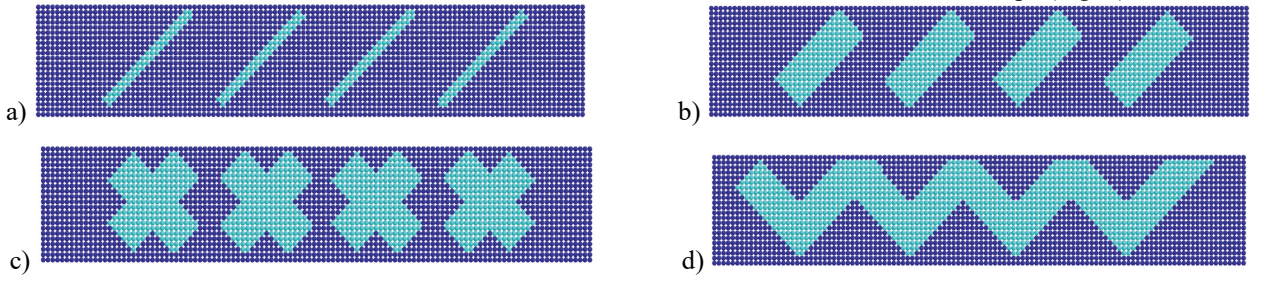

Fig. 4. Cross-sections of the different samples with soft inclusions.

The simulations show that in the case if thin inclusions (Fig. 4,a) the vortex in the velocity field is formed and propagates only in the matrix; the vortex dissipates when it approaches to the inclusion due to plastic deformation of the inclusion material. In the case of thick inclusions (Fig. 4,b and 4,c) the vortex can be formed in the material of inclusion also. The third place where the vortex can be formed is the inclusion-matrix interface. It is interesting to note, that at this time the Mises stress in the inclusion reaches yield limit, and as the vortex propagates forward along the inclusion the Mises stress decreases (Fig. 5). This means that such vortices can be considered as precursors of stress relaxation in nanomaterials in local loading conditions.

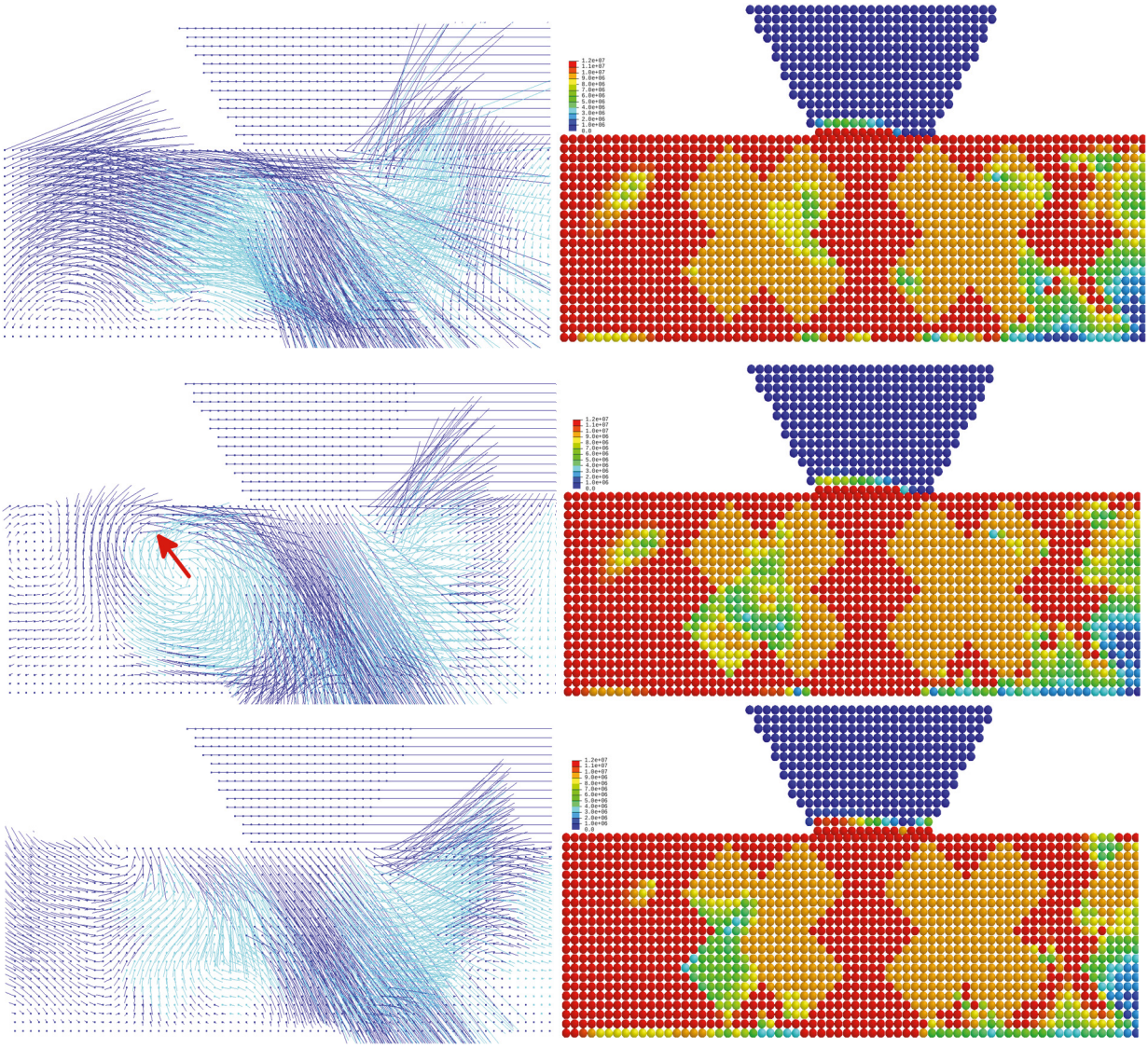

Fig. 5. Velocity field (left) and Mises stress (right) in the cross-section of the sample with thick soft inclusions at different times: before the vortex generation (the upper row), at the vortex propagation (the middle row) and after vortex dissipation (the bottom row).

It has to be noted, that lifetime of the vortices formed and propagating in the elastic matrix is much larger than that in the plastic inclusions. The last one corresponds to the time of elastic wave propagation along the inclusion thickness.

4. Conclusions

Modeling results show that a counter-body sliding on the coating surface generates periodically vortex structures in the coating velocity field. Each of these vortices is located in front of the counter-body at a distance of the contact area radius. Lifetime of the vortex is about the time of sound propagation through the coating height. After this time the vortex vanishes, and then after certain time appears again. Presence of pores and hard inclusions can change the shape and size of the vortex. Presence of weak (plastic) inclusions of extended geometry can lead to vortex generation at the inclusion-matrix interface if the stress in the inclusion reaches yield limit. In this case after propagation of the vortex the stress in the inclusion decreases.

Acknowledgements

The investigation has been carried out at financial support of the Project No. III.23.2.4 (S.G. Psakhie) of the Basic Scientific Research Program of State Academies of Sciences for 2013–2020, and the grant No. 14-19-00718 of the Russian Science Foundation (A.Yu. Smolin, G.M. Eremina, E.V. Shilko).

References

Chertov, M. A., Smolin, A. Yu. , Sapozhnikov, G. A. , Psakhie, S. G., 2004, The Effect of Surface Waves on the Interaction of Incident Particles With a Solid Surface, Technical Physics Letters 30(12), 1009–1012.

Landau, L. D., Lifshitz, E. M., 1970. *Theory of Elasticity, Course in Theoretical Physics*, Vol. 7. Pergamon Press, Oxford.

Lawrence Livermore National Laboratory, VisIt. [online] Available at: < https://wci.llnl.gov/simulation/computer-codes/visit/> [Accessed 11 April 2016].

Levashov, E. A., Petrzhik, M. I., Shtansky, D. V., Kiryukhantsev-Korneev, Ph. V., Sheveyko, A. N., Valiev, R. Z., Gunderov, D. V., Prokoshkin, S. D., Korotitskiy, A. V., Smolin, A. Yu., 2013, Material Science and Engineering A 570, 51–62.

Moiseenko, D. D., Panin, V. E., Elsukova, T. F., 2013, Role of Local Curvature in Grain Boundary Sliding in A Deformed Polycrystal, Physical Mesomechanics 16 (4), 335–347.

Panin, V.E., Egorushkin, V.E., Moiseenko, D.D., Maksimov, P.V., Kulkov, S.N., Panin, S.V., 2016, Functional Role of Polycrystal Grain Boundaries And Interfaces in Micromechanics of Metal Ceramic Composites Under Loading. Computational Materials Science, 116, 74–81.

Psakh'e, S. G., Zol'nikov, K. P., 1997, Anomalously High Rate of Grain Boundary Displacement Under Fast Shear Loading. Technical Physics Letters 23(7), 555–556.

Psakhie, S.G., Smolin, A.Y., Shilko, E.V., Korostelev, S.Y., Dmitriev, A.I., Alekseev, S.V., 1997, About the Features of Transient to Steady State Deformation of Solids, Journal of Materials Science & Technology 13(1), 69-72

Psakhie, S. G., Popov, V. L., Shilko, E. V., Smolin, A. Yu., Dmitriev, A. I., 2009, Spectral Analysis of The Behavior and Properties of Solid Surface Layers. Nanotribospectroscopy, Physical mesomechanics 12(5–6), 221–234.

Psakhie, S. G., Shilko, E. V., Smolin, A. Yu., Dimaki, A. V., Dmitriev, A. I., Konovalenko, Ig. S., Astafurov S. V., Zavshek, S., 2011, Physical Mesomechanics 14(5–6), 224–248.

Psakhie, S. G., Smolin, A. Yu., Shilko, E. V., Anikeeva, G. M., Pogozhev, Yu S., Petrzhik, M. I., Levashov, E. A., 2013, Modeling Nanoindentation of TiCCaPON Coating on Ti Substrate Using Movable Cellular Automaton Method, Computational materials science 76, 89–98.

Psakhie, S. G., Shilko, E. V., Grigoriev, A. S., Astafurov, S. V., Dimaki, A. V., Smolin, A. Yu., 2014a, A Mathematical Model of Particle-Particle Interaction for Discrete Element Based Modeling of Deformation And Fracture of Heterogeneous Elastic-Plastic Materials, Engineering Fracture Mechanics 130, 96–115.

Psakhie, S. G., Zolnikov, K. P., Dmitriev, A. I., Smolin, A. Yu. , Shilko, E. V., 2014b, Dynamic vortex defects in deformed material, Physical Mesomechanics 17(1), 15–22.

Shilko, E.V., Psakhie, S.G., Schmauder, S., Popov, V.L., Astafurov, S.V., Smolin, A.Yu., 2015, Overcoming the limitations of distinct element method for multiscale modeling of materials with multimodal internal structure. Computational materials science 102, 267–285.

Smolin, A.Yu., Roman, N.V., Dobrynin, S.A., Psakhie, S.G., 2009, On rotation in the movable cellular automaton method. Phys Mesomech 12(3–4), 124–9.

Smolin, A.Yu., Shilko, E.V., Astafurov, S.V., Konovalenko, I.S., Buyakova, S.P., Psakhie, S.G., 2015, Modeling mechanical behaviors of composites with various ratios of matrix–inclusion properties using movable cellular automaton method. Defence Techonlogy 11, 18–34.

Yu, Y., Wang, W., He, H., Lu, T., 2014, Modeling Multiscale Evolution of Numerous Voids in Shocked Brittle Material, Physical Review E 89, 043309-1–043309-8

Zhang, Z. F., He, G., Zhang, H., Eckert, J., 2005, Rotation mechanism of shear fracture induced by high plasticity in Ti-based nano-structured composites containing ductile dendrites, Scripta Materialia 52, 945–949.